ACS OMEGA

Open Access

http://pubs.acs.org/journal/acsodf

Article

Noncovalent Interaction-Based Probe Design for PET-Facilitated Fluorescence Sensing of Synthetic Cannabinoids

Jiahao Dong,[#] Chuanfang Zhao,[#] Jinliang Ning, Yuan Liu, and Xincun Dou*

Cite This: *ACS Omega* 2025, 10, 14306−14315

Read Online

ACCESS | Metrics & More | Article Recommendations | Supporting Information

ABSTRACT: Due to the structural diversity and rapid iteration of synthetic cannabinoids (SCs), their detection presents a challenging issue. Here, based on the structure and physicochemical property analysis of a typical SC, MDMB-CHMICA, four fluorescent probes were designed by introducing the recognition groups and fluorescence regulation groups on carbazole. It is found that the electron-withdrawing and conjugation-extending effect of the nitro group reduced the LUMO energy level and thereby narrowed the HOMO−LUMO energy gap, resulting in a red-shift of the fluorescence emission. As a result, the intramolecular charge transfer mechanism of the probe helps to lead to stronger fluorescence with a greater charge transfer distance. Two probes with stronger fluorescence show multiple noncovalent interactions with MDMB-CHMICA and efficient fluorescence quenching sensing through photoinduced electron transfer. This study is expected to shed light on the exploration of fluorescent probes from the analytes' physicochemical nature and would be helpful for new psychoactive substance detection.

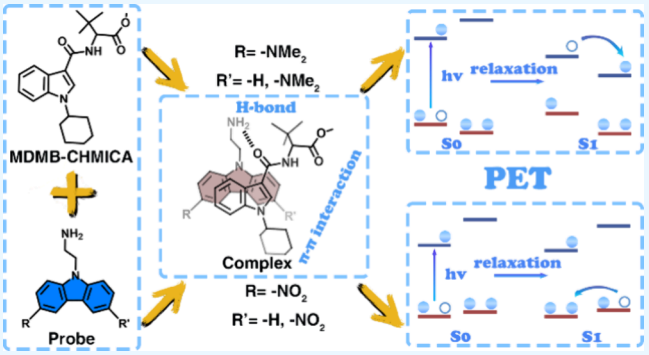

1. INTRODUCTION

Different from the natural first-generation and the chemosynthetic second-generation drugs, new psychoactive substances (NPS) are the third-generation drugs characterized by species diversity, simple synthesis, and rapid iterations.[1] Synthetic cannabinoids (SCs) containing indole, indazole, carbazole, pyrazole, indazole-3-carboxamide, pyrrolo[2,3-*b*]pyridine, and benzimidazole scaffolds are the largest class of NPSs.[2,3] Despite their structural diversity, SCs can function as type 1 cannabinoid receptor (CB1R) agonists, thereby providing pain relief, stimulating appetites, and modulating mood, akin to the effects of Δ9-THC.[4−6] Misuse or overdose of SCs would result in mental euphoria, confusion, dizziness, nausea, vomiting, respiratory depression, cardiovascular disease, acute kidney injury, and potentially fatal outcomes.[7−9] The mental euphoria and addictive nature of SCs has positioned them among the most abused NPS, which has increasingly endangered the health of teenagers, young adults, and marginalized groups.[10,11] Therefore, China and many other countries have enforced strict legal controls over SCs.[12] Meanwhile, SCs' E-liquids are mixed in tobacco, dried flowers, and spices, making it difficult to detect in trace amounts.[13,14] To realize trace detection, a series of methods have been explored, including nuclear magnetic resonance (NMR), liquid chromatography (LC), gas chromatography (GC), GC−mass spectrometry (GC−MS), LC−MS, chips, enzyme-linked immunosorbent assay, electrochemical sensing, and aptamers,[15−17] but most of them require large instruments and/or complicated preprocessing. Visualizing detection methods, such as colorimetric,[18,19] fluorescence,[20−23] or colorimetric-fluorescence dual-mode[24,25] detection methods, are highly promising in-field detection methods, while exploration on the detection of SCs is still rare and demands special effort.

Due to the fact that some NPS are chemically stable and the reactivity of the active sites is rather low, noncovalent interactions have been employed to design some visualizing detection methods. A colorimetric and fluorescent dual-mode probe based on a BODIPY−metal ion complex was developed for synthetic cathinones and γ-hydroxybutyrate (GHB) detection.[26,27] A perylene bisimide-cyclometalated Au(III)-based luminescent film has been designed and used for detecting phenylethylamine sensitively (LOD, <4 ppb) and rapidly (<1 s).[28] Our group also paid special attention to this issue and designed naphthalimide probes for tryptamines and SC JWH-018[29,30] detection and 2-(2′-hydroxyphenyl)benzothiazole probes for GHB detection,[31] with superior fluorescence or colorimetric-fluorescence dual-mode optical responses. Actually, noncovalent interactions comprise a lot of interactions,

Received: January 18, 2025
Revised: March 6, 2025
Accepted: March 26, 2025
Published: April 4, 2025

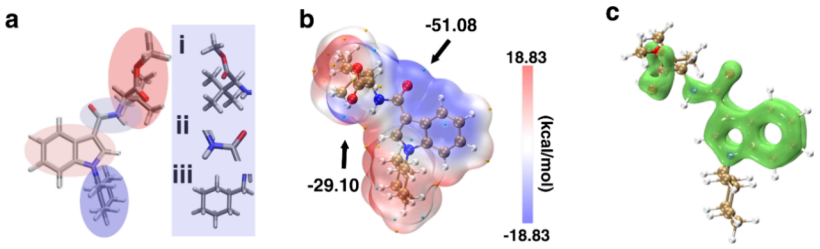

Figure 1. Structure and physicochemical property analysis of MDMB-CHMICA. (a) Structure with (i) the head, (ii) the linker, the core, and (iii) the tail structure, (b) electrostatic potential analysis with the first and second highest values, and (c) LOL-π analysis with the conjugation structure labeled with the continuous green surface.

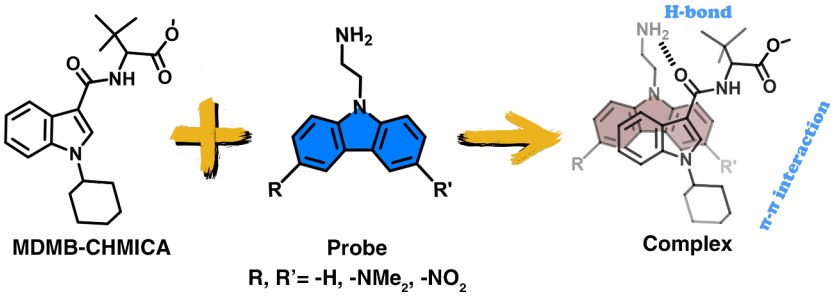

Figure 2. Noncovalent fluorescent probe design by introducing the H-bond donor, hydrophobic groups, or fluorescence modulators with a MDMB-CHMICA-based probe design strategy.

such as electrostatic interaction, hydrogen bond interaction, $\pi\cdots\pi$ interaction, halogen bond interaction, and hydrophobic interaction.[32,33] It is well-known that noncovalent interactions play an important role in molecular science[34−36] and nature and life processes; this is why most of the drugs interact with the human body. For example, SCs bind with its target protein CB1R by forming a $\pi\cdots\pi$ interaction with PHE-170, PHE-200, or PHE-268, forming a hydrophobic interaction with LEU-359 or LEU-387, or forming a hydrogen bond interaction with SER-383.[37,38] Especially, MDMB-CHMICA, with a stronger CB1R agonist (K_i = 0.95 nM, EC_{50} = 21.96 nM) than that of JWH-018 (K_i = 2.69 nM, EC_{50} = 102.8 nM),[39] was reported to be associated with hypoglycemia, recurrent vomiting, asystole, loss of consciousness, seizure adverse effects, and some deaths.[40] However, up to now, no fluorescent probes have been reported for the detection of MDMB-CHMICA (methyl (*R*)-2-(1-(cyclohexylmethyl)-1*H*-indole-3-carboxamido)-3,3-dimethylbutanoate). Thus, whether one can explore a fluorescence method by employing noncovalent interactions for this typical SC structure, especially from the perspective of theoretical calculation and prediction, remains a big challenge.

Herein, with a detailed investigation of the physicochemical properties of MDMB-CHMICA, a series of carbazole-based probes have been designed theoretically to realize fluorescence detection. The carbazole fluorophore, which has ease of modification and fluorescence tuning, was incorporated with the recognition and fluorescence-modulating groups to optimize the sensing performance. It is found that due to the electron-withdrawing and conjugation extension effect of nitro, the carbazole-nitro probes, CSN (2-(3-nitro-9*H*-carbazol-9-yl)-ethan-1-amine) and CDN (2-(3,6-dinitro-9*H*-carbazol-9-yl)-ethan-1-amine), could endow a lower HOMO−LUMO energy gap, a red-shift fluorescence, and a stronger fluorescence strength than the carbazole-amino probes. The carbazole-nitro probes were proven to efficiently recognize MDMB-CHMICA by forming hydrogen bond interaction, $\pi\cdots\pi$ interaction, or hydrophobic interaction and sense it in the form of fluorescence quenching through the photoinduced electron transfer (PET) mechanism. This strategy is expected to pave a way for the exploration of highly efficient fluorescent probes toward analytes that are chemically stable and would help to accelerate the development of fluorescence methods for drug inspection.

2. METHODS

Geometry structures of the carbazole-based probes, MDMB-CHMICA, and their complexes were optimized with the B3LYP/def2-svp method,[41−46] and frequency analysis was carried out with the same method on each optimized structure. Excited state structure optimization and frequency analyses were carried out with the TD-B3LYP/def2-svp method[47,48] and SMD solvation model[49] based on the optimized ground state structures. To compute the excitation energy more precisely, single point energy was computed with the TD-PBE0/def2-tzvp method.[50−53]

To obtain stable binding mode of the probe and MDMB-CHMICA, 2000 conformations were equal-time interval sampled from 10 ns molecular dynamics simulations at 400 K with x-tb software.[54] Subsequently, the 2000 conformations were optimized with the GFN1 method[55] in x-tb, which is launched by Molclus software (Tian Lu, Molclus program, Version 1.10, http://www.keinsci.com/research/molclus.html, Oct. 15th, 2023). The top 10 conformations with the lowest energy were then selected and further optimized with the B3LYP/def2-svp method in Guassian09 software,[56] which is also launched via Molclus. The lowest energy conformation of the probe/MDMB-CHMICA complex was used for further study.

Average local ionization energy (ALIE), local electron affinity energy (LEAE),[57] electrostatic potential,[58] and localized orbital locator (LOL)-π[59] analyses were carried out to study the physicochemical properties of MDMB-CHMICA and carbazole-based probes. To study their recognition mechanism, independent gradient model (IGM)[60] analyses were carried out

https://doi.org/10.1021/acsomega.5c00540
ACS Omega 2025, 10, 14306−14315

on the optimized probe/MDMB-CHMICA complex. To gain insight into their luminescence mechanism, frontier molecular orbital population analyses and electron−hole distribution analyses were performed on the optimized probe and probe/MDMB-CHMICA complex. All the quantum computations were performed with Gaussian09 software, wavefunction analyses were carried out with Multiwfn software,[61,62] and pictures were generated with VMD software.[63]

3. RESULTS AND DISCUSSION

3.1. Structure and Physicochemical Property Analyses of MDMB-CHMICA. Before designing the probes, we conducted a detailed computational study on the structure and physicochemical properties of MDMB-CHMICA. Structure analyses showed that MDMB-CHMICA consists of a 3,3-dimethyl butanoic methyl ester head, an amide linker, an indole core, and a cyclohexyl tail (Figure 1a). The hydrophobicity and steric hindrance of the head and tail made MDMB-CHMICA insoluble in water (lg P = 4.911).

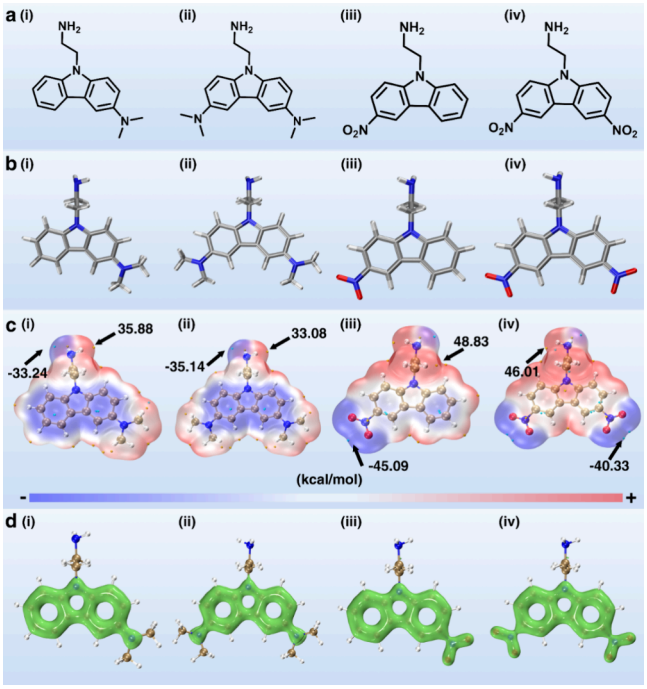

Figure 3. Structure and physicochemical property analyses of newly designed fluorescent probes: (i) CSD, (ii) CDD, (iii) CSN, and (iv) CDN. (a) 2D structure, (b) the optimized 3D structure, (c) electrostatic potential analysis with the highest and lowest values, and (d) LOL-π analysis with conjugation structures labeled as the continuous green surface.

Electrostatic potential analysis indicated that electrons mainly distributed on the indole core and the oxygen atom of the amide linker and ester head (Figure 1b). This is verified by the atomic charge analyses (Figure S1a), in which the heavy atoms in the indole and the oxygen atoms in both amide and ester groups have negative atomic charge. The local electrostatic potential values near the oxygen atoms in both ester and amide groups are −29.10 and −51.08 kcal/mol, respectively, implying that they can serve as hydrogen bond acceptors.

The LOL-π analysis indicated that the amide linker is conjugated with the indole core (Figure 1c), in which the electron-withdrawing effect of the amide carboxyl increased the electron density on it, making the oxygen electrostatic potential of the amide (−51.08 kcal/mol) significantly lower than that of the ester (−29.10 kcal/mol). Frontier molecular orbital analyses indicated that MDMB-CHIMICA has a HOMO−LUMO energy gap of 5.24 eV (Figure S1b), suggesting that it is less prone to excitation. ALIE and LEAE computational results showed that the electrophilic and nucleophilic reaction sites are located on the indole of MDMB-CHMICA (Figure S1c,d), for which the reaction condition is harsh, requiring heating or a catalyst.[64] Therefore, it is hard to develop covalent probes for the detection of MDMB-CHMICA.

3.2. Fluorescent Probe Design Based on the Structure Analysis of MDMB-CHMICA. Guided by the physicochemical property analyses of MDMB-CHMICA, some noncovalent florescent probes were designed. Carbazole was employed as the fluorophore moiety of the probes owing to its high fluorescence quantum yield, ease of modification, and tunable fluorescence color. Four carbazole-based fluorescent probes were designed by incorporating hydrogen bond donor/acceptor functionalities, hydrophobic groups, or electron-donating/withdrawing groups into their structure (Figure 2). Just like the key residues in CB1R, these groups were expected to form a hydrogen bond interaction, $\pi\cdots\pi$ interaction, or hydrophobic interactions with MDMB-CHMICA.

The 2-aminoethyl group on N9 (CEA, Figure S2a), one or two dimethyl amino groups (CSD, CDD), or nitro groups (CSN, CDN) on C3 and/or C6 of carbazole were introduced in the design of these fluorescent probes, shown in the 2D and optimized 3D structures (Figure 3a,b). With further electrostatic potential analyses (Figure 3c), the maximum (35.88, 33.08 kcal/mol) and minimum values (−33.24, −35.14 kcal/mol) of the electrostatic potential located nearby the hydrogen and nitrogen atoms of the amino group in CSD and CDD. However, in CSN and CDN, the maximum (48.83, 46.01 kcal/mol) and minimum values (−45.09, −40.33 kcal/mol) of the electrostatic potential located nearby the hydrogen atom of the amino group and oxygen atom of the nitro group. Compared with those of CSD and CDD, the electron density on carbazole is reduced significantly in CSN and CDN. To investigate the impact of the substituent on electron distribution within probes, the atomic charges were calculated with the Merz−Kollmann-based RESP (Restrained Electrostatic Potential) method (Figure S2b).[65] The atomic charge computational analyses showed that in CSD and CDD, the nitrogen atom in the amino group exhibited the most negative charge, while the hydrogen atom in the same group displayed the most positive charge (Figure S3a,b). This result is different from those of CSN and CDN, in which the oxygen atom in the nitro group exhibited the most negative charge and the hydrogen atom in the amino group displayed the most positive charge (Figure S3c,d). This atomic charge computational result is consistent with that of the electrostatic potential analysis. To investigate the effect of substituents on the conjugation degree of the probes, LOL-π analyses were carried out (Figure 3d). It is shown that compared to CEA (Figure S4a), introducing the dimethylamino or nitro groups extended the conjugation system. In CSD and CDD, the nitrogen atom of dimethylamino conjugated with carbazole, while in CSN and CDN, the nitro groups conjugated with carbazole. Thus, the electron-withdrawing induction and conjugation effects of the nitro group transformed the carbazole moiety from an electron-rich (CEA, CSD, and CDD) group to an electron-poor (CSN and CDN) group.

https://doi.org/10.1021/acsomega.5c00540
ACS Omega 2025, 10, 14306−14315

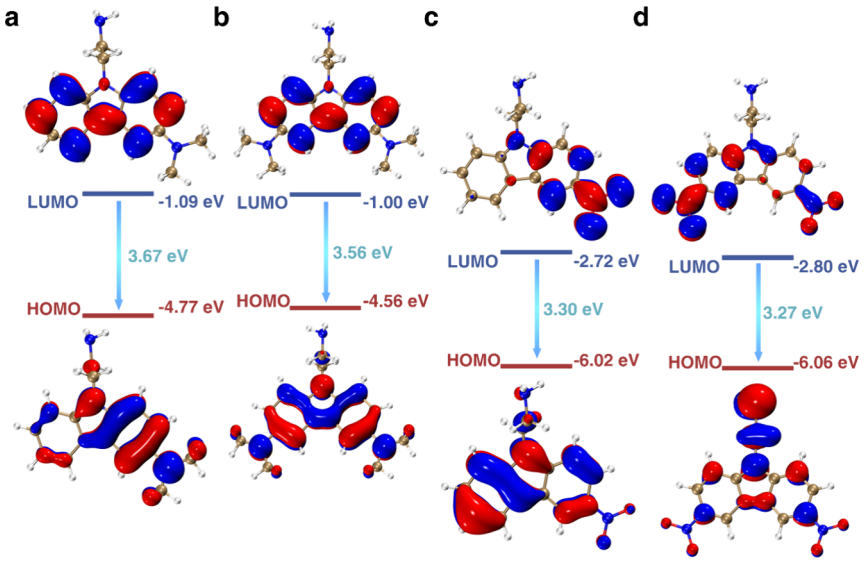

Figure 4. Frontier orbital analyses of the newly designed probes in the S1 state: (a) CSD, (b) CDD, (c) CSN, and (d) CDN.

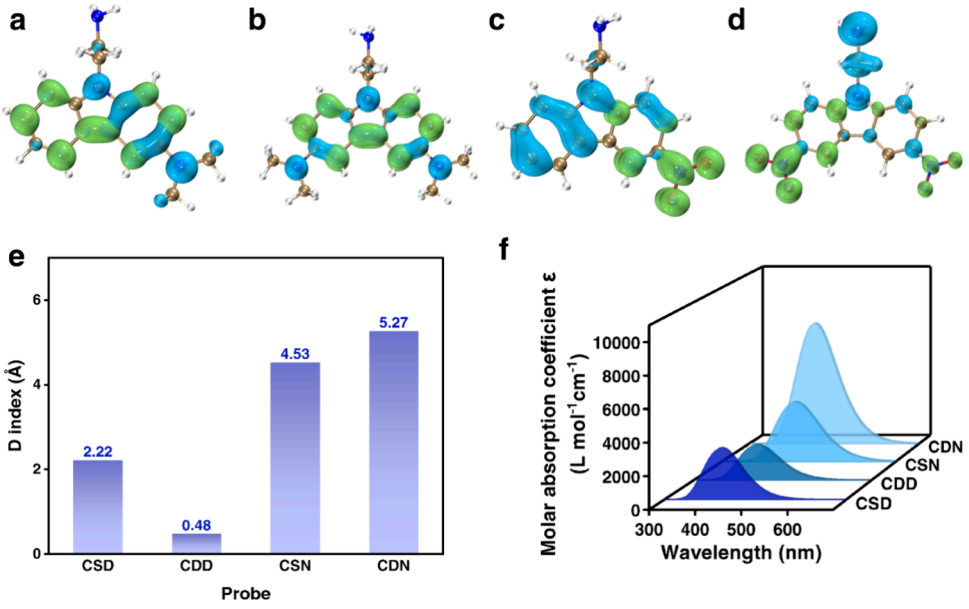

Figure 5. Electron−hole analysis of the probes (a) CSD, (b) CDD, (c) CSN, and (d) CDN in the S1 state with electrons and holes denoted as green and blue, respectively, (e) D index (the charge transfer distance), and (f) theoretical fluorescence spectrum comparison.

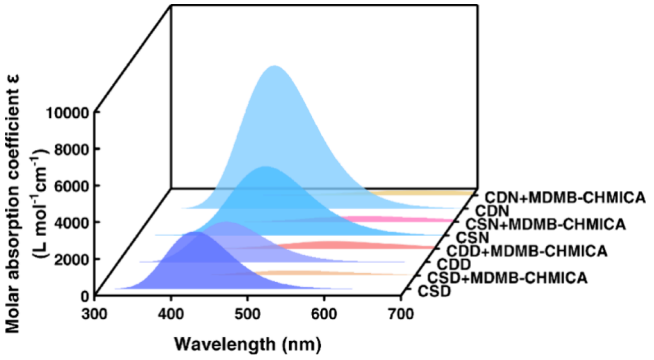

Figure 6. Simulated fluorescence of the probes and the probe/MDMB-CHMICA complexes.

The frontier molecular orbital analyses indicated that in probes CSD and CDD, the HOMO localized on the amino and carbazole groups and the LUMO localized on the carbazole moiety (Figure 4a,b). Meanwhile, in CSN and CDN, the HOMO distributed on carbazole and 2-aminoethyl groups and the LUMO distributed on carbazole and nitro groups (Figure 4c,d). The HOMO−LUMO energy gap for CSD, CDD, CSN, and CDN were obtained with values of 3.67, 3.56, 3.30, and 3.27 eV, respectively. In contrast to CEA (4.55 eV in Figure S4b), the introduction of the amino or nitro groups onto carbazole resulted in a reduction of the HOMO−LUMO energy gap due to the conjugation extending effect. Thus, the electron-withdrawing and conjugation extending effect of the nitro groups decreased the LUMO energy of probes CSN and CDN further, thus reducing their HOMO−LUMO energy gap, which is lower than those of CSD and CDD.

https://doi.org/10.1021/acsomega.5c00540
ACS Omega 2025, 10, 14306−14315

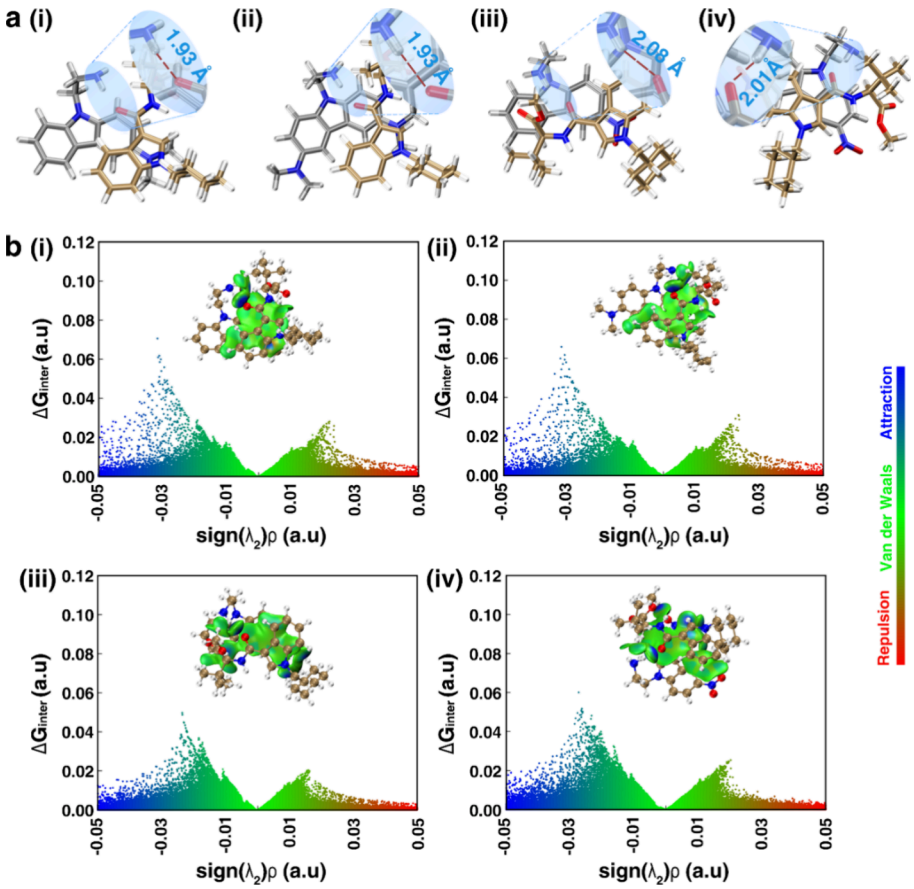

Figure 7. Binding interactions of the four probes ((i) CSD, (ii) CDD, (iii) CSN, and (iv) CDN) and MDMB-CHMICA (a) and (b) IGM analyses of the probe/MDMB-CHMICA complex.

Electron−hole distribution analyses indicated that in the excited state of CSD and CDD, the hole is distributed on the amino group and part of the carbazole and the electron is distributed across the remaining part of the carbazole (Figure 5a,b). Thus, after excitation, electrons transfer from the electron-donating amino group and part of the carbazole to the other part of the carbazole. Meanwhile, in CSN and CDN, the electron is distributed on nitro and part of carbazole, and the hole is distributed on the other part of carbazole and the 2-aminoethyl group. Therefore, after excitation, electrons transfer from the part of carbazole and the 2-aminoethyl group to the other part of carbazole and the nitro group (Figure 5c,d). Thus, it is clear that all the luminescence mechanisms for CSD, CDD, CSN, and CDN can be confirmed as intramolecular charge transfer.

Furthermore, it is observed that the charge transfer distances (D index) of CDD, CSD, CSN, and CDN vary with values of 0.48, 2.22, 4.53, and 5.27 Å, respectively (Figure 5e). Through further analyses of the oscillator strengths of CDD, CSD, CSN, and CDN of 0.05, 0.08, 0.09, and 0.19, respectively (Table S1), as well as the fluorescence strength (Figure 5f), it is found that the larger the charge transfer distance, the stronger the fluorescence, and the fluorescence of CSN and CDN is the strongest.

It is observed that the fluorescence emissions of CSD, CDD, CSN, and CDN center at 425.13, 441.08, 467.61, and 453.92 nm, respectively, which resulted from the change of the HOMO−LUMO energy gaps; the smaller the HOMO−LUMO energy gap, the longer the fluorescence emission wavelength.

3.3. Recognition and Sensing Mechanism for Detecting MDMB-CHMICA. Compared with probes, the oscillator strength of probe/MDMB-CHMICA complexes reduced significantly, equal to or less than 0.01, which implies that all of the probes could detect MDMB-CHMICA through the fluorescence-quenching mode (Figure 6, Tables S1−S2). This result has been evidenced by the experimental data, in which the CSN probe showed an emission centered at 514 nm with a fluorescence intensity of 6×10^4, while it red-shifted to 530 nm with the intensity reduced to 9×10^3 after binding with MDMB-CHMICA (Figure S5−8). It is clear that due to the intrinsically strong fluorescence, CSN and CDN showed a much more pronounced fluorescence quenching and are considered to be more promising probes for detecting MDMB-CHMICA.

To investigate the recognizing and sensing mechanism of these probes for detecting MDMB-CHMICA, the binding interaction and electronic properties of probe/MDMB-CHMICA complexes were investigated by using DFT and TD-DFT methods.

IGM analyses indicated that CSD and CDD bound with MDMB-CHMICA by forming a hydrogen bond interaction with the oxygen of amide, forming a $\pi\cdots\pi$ interaction with the indole-amide group, and a hydrophobic interaction with cyclohexyl (Figure 7a,b). CSN and CDN formed a hydrogen bond interaction with the oxygen of amide, formed a $\pi\cdots\pi$ interaction with the indole-amide group, and formed a weak hydrogen bond interaction between the oxygen of nitro and the H−C of the cyclohexyl of MDMB-CHMICA. These multiple noncovalent interactions drove probes to recognize and bind to

https://doi.org/10.1021/acsomega.5c00540
ACS Omega 2025, 10, 14306−14315

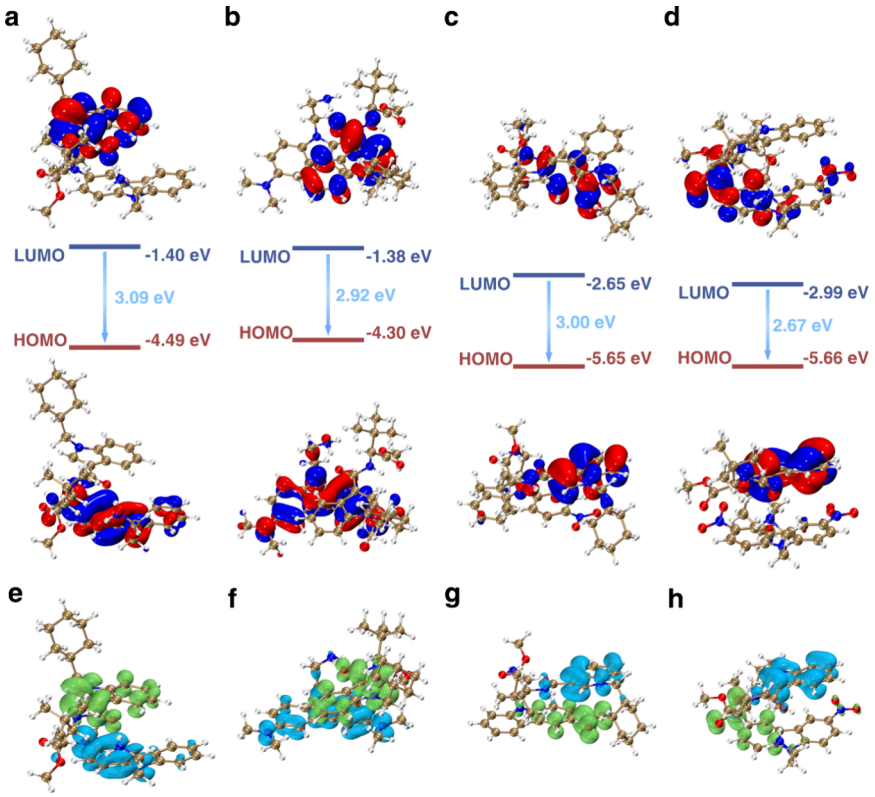

Figure 8. Frontier molecular orbitals (a−d) and electron−hole (e−h) analyses of four probes (CSD (a, e), CDD (b, f), CSN (c, g), CDN (d, h)) and MDMB-CHMICA complexes.

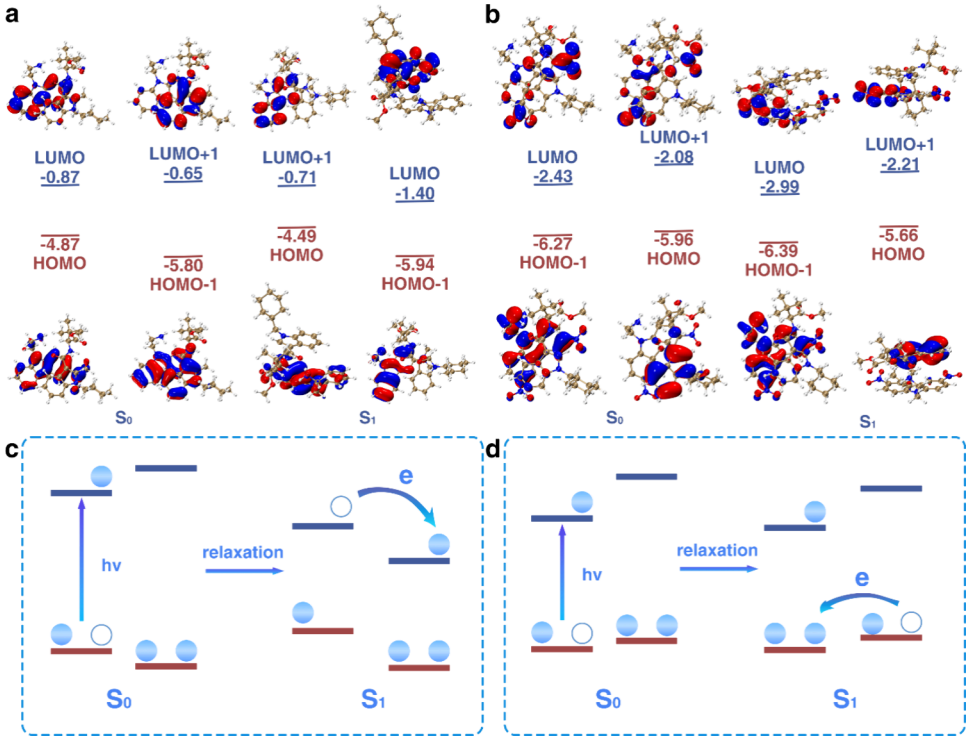

Figure 9. Frontier molecular orbital analyses of (a) CSD/MDMB-CHMICA and (b) CDN/MDMB-CHMICA complexes in ground (S_0) and excited states (S_1). Schematic diagrams of the electron transfer mechanisms for the complexes of (c) carbazole-amino and (d) carbazole-nitro probes and MDMB-CHMICA.

MDMB-CHMICA with binding energies of CSD, CDD, CSN, and CDN of −9.80, −10.76, −7.67, and −12.24 kcal/mol (Table S3), respectively, and CDN/MDMB-CHMICA reveals to be the most stable complex. This may be correlated to its high fluorescence quenching efficacy.

https://doi.org/10.1021/acsomega.5c00540
ACS Omega 2025, 10, 14306−14315

Frontier molecular orbital analyses indicated that in the complex of CSD, CDD and MDMB-CHMICA (Figure 8a,b), the HOMO orbital located on the carbazole-amino group of the probe and the LUMO orbital located on the indole-amide group of MDMB-CHMICA. This result is different from the complexes of CSN, CDN and MDMB-CHMICA (Figure 8c,d), in which the HOMO is mainly distributed on the indole-amide group of MDMB-CHMICA and the LUMO is distributed on the carbazole-nitro group. The HOMO−LUMO energy gaps of the complexes of CDD, CSD, CSN, CDN and MDMB-CHMICA were calculated to be 3.09, 2.92, 3.00, and 2.67 eV, respectively. Thus, by introducing the electron-withdrawing group onto the carbazole of the probe decreased the LUMO energy of the complex and thus decreased the HOMO−LUMO energy gap, in which CDN possesses the lowest HOMO−LUMO energy gap.

Furthermore, the electron−hole distribution analyses showed that in the complexes of CSD, CDD and MDMB-CHMICA (Figure 8e,f), electrons mainly distributed on the indole-amide group of MDMB-CHMICA and holes distributed on the carbazole-amino group of the probe. Thus, in the excited state of the carbazole-amino probe/MDMB-CHMICA complex, an electron transferred from the probe to MDMB-CHMICA. This result is different from that of the carbazole-nitro probe/MDMB-CHMICA complexes (Figure 8g,h), in which electrons distributed on the carbazole-nitro group of the probe (CSN, CDN), holes distributed on the indole-amide group of MDMB-CHMICA, and, in the excited state, electrons transfer from MDMB-CHMICA to the carbazole-nitro probe. Therefore, these fluorescent probes detected MDMB-CHMICA through PET-facilitated fluorescence quenching.

Further frontier molecular orbital analyses indicated that in the ground state (S_0, Figure 9a), the HOMO and LUMO of the CSD/MDMB-CHMICA complex are mainly located on the probe. Meanwhile, in the excited state (S_1), the LUMO energy of MDMB-CHMICA (−1.40 eV) decreased, which is lower than that of the probe (−0.71 eV), while in the S_0 of the CDN/MDMB-CMICA complex (Figure 9b), the HOMO−LUMO energy gap of CDN (3.84 eV) is lower than that of MDMB-CHMICA (3.88 eV). Due to the intramolecular electron excitation prior to intermolecular excitation, the electrons would be excited from the HOMO of the probe to its LUMO. Meanwhile, in the S_1 state, the HOMO energy of the probe (−6.39 eV) is lower than the HOMO energy of MDMB-CHMICA (−5.66 eV).

Thus, for the probes with carbazole-amino groups, the excited electrons would transfer from the probe LUMO to the MDMB-CHMICA LUMO and form a relatively stable S_1 state, resulting in electrons transferring from the probe to MDMB-CHMICA (Figure 9c). For the probes with carbazole-nitro groups, the electrons would transfer from the HOMO of MDMB-CHMICA to the HOMO of the probe, forming a relatively stable S_1 state, leading to electrons transferring from MDMB-CHMICA to the probe (Figure 9d).

The PET mechanism and the molecular orbital energy analyses indicate that the electron transfer driving force of MDMB-CHMICA in complex with CSD or CDD could be the LUMO−LUMO + 1 energy gap with a value of 0.69 or 0.45 eV, while that of MDMB-CHMICA in complex with CSN or CDN could be attributed to the HOMO − 1−HOMO energy gap with a value of 0.41 or 0.73 eV (Table S4). Thus, the complex CDN/MDMB-CHMICA, which has the largest electron transfer driving force, is expected to have the highest fluorescence quenching efficiency.

Therefore, it is clearly demonstrated that the carbazole-based probes detected MDMB-CHMICA through PET-facilitated fluorescence quenching. Due to the strongest binding interaction with MDMB-CHMICA and the largest electron transfer driving force of the CDN/MDMB-CHMICA complex with the PET process, the CDN probe with the highest fluorescence intensity is predicted to have the highest fluorescence quenching efficiency.

CONCLUSIONS

In summary, facing with the challenging issue of how to effectively utilize the noncovalent interactions for fluorescence sensing of chemically stable analytes, we proposed an efficient probe design strategy based on the theoretical analysis of the physicochemical properties of the target molecules. Four carbazole-based probes have been designed for fluorescence sensing of MDMB-CHMICA. It is found that the electron-withdrawing and conjugation extending effect of the nitro group would decrease the LUMO energy level and thereby narrow the HOMO−LUMO energy gap of probes and thus lead to the red-shift of the fluorescence emission. Driven by the multiple noncovalent interactions, these probes could recognize MDMB-CHMICA and sense it through PET-facilitated fluorescence quenching. CSN and CDN were theoretically predicted to exhibit strong fluorescence, and on binding with MDMB-CHMICA, they could manifest a remarkable fluorescence emission change. We hope that the present fluorescent probe design strategy considering the physicochemical properties of the targets and the theoretical perspective would greatly advance the experimental development of functional probes.

ASSOCIATED CONTENT

Supporting Information

The Supporting Information is available free of charge at https://pubs.acs.org/doi/10.1021/acsomega.5c00540.

Experimental methods; physicochemical property analyses of MDMB-CHMICA; structure and the M-K atomic charge analyses of CEA; the M-K atomic charge analysis of CSD, CDD, CSN, and CDN; the LOL-π analysis and the HOMO-LUMO analysis of CEA; the synthesis route of the CSN probe; HRMS spectrum of the CSN probe; ^{1}H NMR spectrum of the CSN probe; the emission spectra of the CSN probe and the CSN/MDMB-CHMICA complex; the fluorescence wavelength, molar absorption coefficient, and oscillator strength of the four probes; the fluorescence wavelength, molar absorption coefficient, and oscillator strength of the probe/MDMB-CHMICA complexes; the binding energy of the probe/MDMB-CHMICA complexes; the driving force of PET of the probe/MDMB-CHMICA complexes (PDF)

AUTHOR INFORMATION

Corresponding Author

Xincun Dou − *School of Materials Science and Engineering, Xinjiang University, Urumqi, Xinjiang 830046, China; Xinjiang Key Laboratory of Trace Chemical Substances Sensing, Xinjiang Joint Laboratory of Illicit Drugs Control, Xinjiang Technical Institute of Physics and Chemistry, Chinese Academy of Sciences, Urumqi 830011, China; Center of Materials Science and Optoelectronics Engineering, University*

https://doi.org/10.1021/acsomega.5c00540
ACS Omega 2025, 10, 14306−14315

of Chinese Academy of Sciences, Beijing 100049, China; orcid.org/0000-0001-5825-9937; Email: xcdou@ms.xjb.ac.cn

Authors

Jiahao Dong − *School of Materials Science and Engineering, Xinjiang University, Urumqi, Xinjiang 830046, China*

Chuanfang Zhao − *Xinjiang Key Laboratory of Trace Chemical Substances Sensing, Xinjiang Joint Laboratory of Illicit Drugs Control, Xinjiang Technical Institute of Physics and Chemistry, Chinese Academy of Sciences, Urumqi 830011, China*

Jinliang Ning − *Xinjiang Key Laboratory of Trace Chemical Substances Sensing, Xinjiang Joint Laboratory of Illicit Drugs Control, Xinjiang Technical Institute of Physics and Chemistry, Chinese Academy of Sciences, Urumqi 830011, China; Center of Materials Science and Optoelectronics Engineering, University of Chinese Academy of Sciences, Beijing 100049, China*

Yuan Liu − *Xinjiang Key Laboratory of Trace Chemical Substances Sensing, Xinjiang Joint Laboratory of Illicit Drugs Control, Xinjiang Technical Institute of Physics and Chemistry, Chinese Academy of Sciences, Urumqi 830011, China; Center of Materials Science and Optoelectronics Engineering, University of Chinese Academy of Sciences, Beijing 100049, China*

Complete contact information is available at: https://pubs.acs.org/10.1021/acsomega.5c00540

Author Contributions

#Jiahao Dong and Chuanfang Zhao contributed equally to this work.

Notes

The authors declare no competing financial interest.

■ ACKNOWLEDGMENTS

This work was funded by the Key Research and Development Program of Xinjiang (2023B03021), Tianshan Innovation Team Plan (2024D14019), and the Tianchi Talent Plan.

■ REFERENCES

(1) Peacock, A.; Bruno, R.; Gisev, N.; Degenhardt, L.; Hall, W.; Sedefov, R.; White, J.; Thomas, K. V.; Farrell, M.; Griffiths, P. New psychoactive substances: challenges for drug surveillance, control, and public health responses. *Lancet* **2019**, *394* (10209), 1668−1684.

(2) Skinnider, M. A.; Wang, F.; Pasin, D.; Greiner, R.; Foster, L. J.; Dalsgaard, P. W.; Wishart, D. S. A deep generative model enables automated structure elucidation of novel psychoactive substances. *Nat. Mach. Intell.* **2021**, *3* (11), 973−984.

(3) Abdollahzadeh Hamzekalayi, M. R.; Hooshyari Ardakani, M.; Moeini, Z.; Rezaei, R.; Hamidi, N.; Rezaei Somee, L.; Zolfaghar, M.; Darzi, R.; Kamalipourazad, M.; Riazi, G.; et al. A systematic review of novel cannabinoids and their targets: Insights into the significance of structure in activity. *Eur. J. Pharmacol.* **2024**, *976*, No. 176679.

(4) Liao, Y.-Y.; Zhang, H.; Shen, Q.; Cai, C.; Ding, Y.; Shen, D.-D.; Guo, J.; Qin, J.; Dong, Y.; Zhang, Y.; et al. Snapshot of the cannabinoid receptor 1-arrestin complex unravels the biased signaling mechanism. *Cell* **2023**, *186* (26), 5784−5797.

(5) Hua, T.; Li, X.; Wu, L.; Iliopoulos-Tsoutsouvas, C.; Wang, Y.; Wu, M.; Shen, L.; Brust, C. A.; Nikas, S. P.; Song, F.; et al. Activation and signaling mechanism revealed by cannabinoid receptor-G_i complex structures. *Cell* **2020**, *180* (4), 655−665.

(6) Hua, T.; Vemuri, K.; Nikas, S. P.; Laprairie, R. B.; Wu, Y.; Qu, L.; Pu, M.; Korde, A.; Jiang, S.; Ho, J.-H.; et al. Crystal structures of agonist-bound human cannabinoid receptor CB1. *Nature* **2017**, *547* (7664), 468−471.

(7) Patel, M.; Zheng, X.; Akinfiresoye, L. R.; Prioleau, C.; Walker, T. D.; Glass, M.; Marusich, J. A. Pharmacological evaluation of new generation OXIZID synthetic cannabinoid receptor agonists. *Eur. J. Pharmacol.* **2024**, *971*, No. 176549.

(8) Glatfelter, G. C.; Partilla, J. S.; Baumann, M. H. Structure-activity relationships for 5F-MDMB-PICA and its 5F-pentylindole analogs to induce cannabinoid-like effects in mice. *Neuropsychopharmacol.* **2022**, *47* (4), 924−932.

(9) Zagzoog, A.; Brandt, A. L.; Black, T.; Kim, E. D.; Burkart, R.; Patel, M.; Jin, Z.; Nikolaeva, M.; Laprairie, R. B. Assessment of select synthetic cannabinoid receptor agonist bias and selectivity between the type 1 and type 2 cannabinoid receptor. *Sci. Rep.* **2021**, *11* (1), 10611.

(10) Engelgardt, P.; Krzyżanowski, M.; Borkowska-Sztachańska, M.; Wasilewska, A.; Ciucias, M. Life time use of illicit substances among adolescents and young people hospitalized in psychiatric hospital. *Sci. Rep.* **2023**, *13* (1), 1866.

(11) Miliano, C.; Margiani, G.; Fattore, L.; De Luca, M. A. Sales and advertising channels of new psychoactive substances (NPS): Internet, social networks, and smartphone apps. *Brain Sci.* **2018**, *8* (7), 123.

(12) Huang, Y.; Jia, W.; Chen, Y.; Liu, C.; Liu, S.; Su, M.; Hua, Z. A comprehensive analytical strategy based on characteristic fragments to detect synthetic cannabinoid analogs in seized products and hair samples. *Talanta* **2023**, *265*, No. 124830.

(13) Magny, R.; Lefrère, B.; Roulland, E.; Auzeil, N.; Farah, S.; Richeval, C.; Gish, A.; Vodovar, D.; Labat, L.; Houzé, P. Feature-based molecular network for new psychoactive substance identification: The case of synthetic cannabinoids in a seized e-liquid and biological samples. *J. Am. Soc. Mass Spectrom.* **2024**, *35* (10), 2276−2287.

(14) Fan, Y.; Zong, X.; Liu, J.; Ke, X.; Huang, Z.; Xu, Y. J. Development of a fragmentation pattern of synthetic cannabinoids based on electrospray ionization mass spectrometry in positive ion mode to screen synthetic cannabinoids in illicit products. *J. Pharm. Biomed. anal.* **2021**, *193*, No. 113723.

(15) Dronova, M.; Smolianitski, E.; Lev, O. Electrooxidation of new synthetic cannabinoids: Voltammetric determination of drugs in seized street samples and artificial saliva. *Anal. Chem.* **2016**, *88* (8), 4487−4494.

(16) Santos, A. D. C.; Dutra, L. M.; Menezes, L. R. A.; Santos, M. F. C.; Barison, A. Forensic NMR spectroscopy: Just a beginning of a promising partnership. *Trac-Trends Anal. Chem.* **2018**, *107*, 31−42.

(17) Lin, M.; Lee, J. C.; Blake, S.; Ellis, B.; Eubanks, L. M.; Janda, K. D. Broadly neutralizing synthetic cannabinoid vaccines. *JACS Au* **2021**, *1* (1), 31−40.

(18) Treto-Suárez, M. A.; Tapia, J.; Hidalgo-Rosa, Y.; Páez-Hernández, D.; Molins, E.; Zarate, X.; Schott, E. New sensitive and selective chemical sensors for Ni^{2+} and Cu^{2+} ions: Insights into the sensing mechanism through DFT methods. *J. Phys. Chem. A* **2020**, *124* (32), 6493−6503.

(19) Hu, X.; Zhang, T.; Li, J.; Ma, Z.; Lei, D.; Zu, B.; Dou, X. Competitive delocalized charge transfer boosted by solvent induction strategy for survivable colorimetric detection of ng-level urea. *Anal. Chem.* **2022**, *94* (16), 6318−6328.

(20) Bhat, H. R.; Rana, M. K.; Dar, A. A. Sensing cyclosarin (a chemical warfare agent) by Cucurbit[n]urils: A DFT/TD-DFT study. *J. Mol. Struct.* **2023**, *1272*, No. 134163.

(21) Ke, Y.; Liu, Y.; Zu, B.; Lei, D.; Wang, G.; Li, J.; Ren, W.; Dou, X. Electronic tuning in reaction-based fluorescent sensing for instantaneous and ultrasensitive visualization of ethylenediamine. *Angew. Chem., Int. Ed.* **2022**, *61* (29), No. e202203358.

(22) Xu, W.-Z.; Song, L.; Jin, H.-X.; Jin, D.-F.; Wei, X.-Y.; Zhang, Y.-X.; Shen, H.-Y.; Chai, W.-X. A luminescent binuclear Cu(I) complex constructed by bipyridine, TD-DFT calculation, and its fluorescent sensing properties for VOCs. *J. Mol. Struct.* **2024**, *1318*, No. 139283.

(23) Miao, X.; Wu, C.; Xia, Y.; Yu, S.; Li, F.; Zhang, M. Ratiometric fluorescence probes for visible detection and accurate identification of MPEA vapor. *Nat. Commun.* **2024**, *15* (1), 10641.

(24) Zhang, T.; Liu, Y.; Li, J.; Ren, W.; Dou, X. High-performance fluorescent and colorimetric dual-mode nitrite sensor boosted by a

versatile coumarin probe equipped with diazotization-coupling reaction-sites. *Sens. Actuat. B-Chem.* **2023**, *379*, No. 133261.
(25) Su, Z.; Li, Y.; Li, J.; Li, K.; Dou, X. Ultrasensitive dual-mode visualization of perchlorate in water, soil and air boosted by close and stable Pt−Pt packing endowed low-energy absorption and emission. *J. Mater. Chem. A* **2022**, *10* (15), 8195−8207.
(26) Hernández-Contreras, J.; Parra, M.; Gil, S.; Costero, A. M.; Arroyo, P.; Sancenón, F.; Martínez-Máñez, R.; Sáez, J. A.; Gaviña, P. Colorimetric and fluorescent detection of synthetic cathinones in oral fluid with meso-aryl BODIPYs and Cu(II). *RSC Adv.* **2022**, *12* (44), 28580−28585.
(27) Ryu, J.; Kim, Y. Overcoming interferences in the colorimetric and fluorimetric detection of γ-hydroxybutyrate in spiked beverages. *Sens. Actuat. B-Chem.* **2022**, *364*, No. 131861.
(28) Zhang, J.; Shi, Z.; Liu, K.; Shi, Q.; Yi, L.; Wang, J.; Peng, L.; Liu, T.; Ma, M.; Fang, Y. Fast and selective luminescent sensing by langmuir−schaeffer films based on controlled assembly of perylene bisimide modified with a cyclometalated Au^{III} complex. *Angew. Chem., Int. Ed.* **2023**, *62* (52), No. e202314996.
(29) Liu, C.; Xiao, F.; Li, Y.; Lei, D.; Liu, Y.; Ma, X.; Gu, C.; Dou, X. Intermolecular through-space charge transfer enabled by bicomponent assembly for ultrasensitive detection of synthetic cannabinoid JWH-018. *Aggregate* **2023**, *4* (4), No. e315.
(30) Pang, L.; Zhang, T.; Liu, Y.; Li, D.; Li, J.; Guan, M.; Dou, X. Dual noncovalent interaction facilitated highly sensitive and specific colorimetric−fluorescent sensing for tryptamines. *Sens. Actuat. B-Chem.* **2023**, *391*, No. 134061.
(31) Zhang, S.; Liu, Y.; Dong, J.; Li, J.; Lei, D.; Dou, X. Electronic effect driven specific and sensitive recognition toward GHB. *Anal. Chem.* **2024**, *96* (22), 9026−9033.
(32) Qu, D.-H.; Wang, Q.-C.; Zhang, Q.-W.; Ma, X.; Tian, H. Photoresponsive host−guest functional systems. *Chem. Rev.* **2015**, *115* (15), 7543−7588.
(33) Liu, H.-W.; Chen, L.; Xu, C.; Li, Z.; Zhang, H.; Zhang, X.-B.; Tan, W. Recent progresses in small-molecule enzymatic fluorescent probes for cancer imaging. *Chem. Soc. Rev.* **2018**, *47* (18), 7140−7180.
(34) Zhao, Z.; Zhang, H.; Lam, J. W. Y.; Tang, B. Z. Aggregation-induced emission: New vistas at the aggregate level. *Angew. Chem., Int. Ed.* **2020**, *59* (25), 9888−9907.
(35) Tu, Y.; Zhao, Z.; Lam, J. W. Y.; Tang, B. Z. Aggregate science: Much to explore in the meso world. *Matter* **2021**, *4* (2), 338−349.
(36) He, W.; Kwok, R. T. K.; Qiu, Z.; Zhao, Z.; Tang, B. Z. A holistic perspective on living aggregate. *J. Am. Chem. Soc.* **2024**, *146* (8), 5030−5044.
(37) Yang, X.; Wang, X.; Xu, Z.; Wu, C.; Zhou, Y.; Wang, Y.; Lin, G.; Li, K.; Wu, M.; Xia, A.; et al. Molecular mechanism of allosteric modulation for the cannabinoid receptor CB1. *Nat. Chem. Biol.* **2022**, *18* (8), 831−840.
(38) Krishna Kumar, K.; Shalev-Benami, M.; Robertson, M. J.; Hu, H.; Banister, S. D.; Hollingsworth, S. A.; Latorraca, N. R.; Kato, H. E.; Hilger, D.; Maeda, S.; et al. Structure of a signaling cannabinoid receptor 1-G protein complex. *Cell* **2019**, *176* (3), 448−458.
(39) Münster-Müller, S.; Hansen, S.; Lucas, T.; Giorgetti, A.; Mogler, L.; Fischmann, S.; Westphal, F.; Auwärter, V.; Pütz, M.; Opatz, T. Synthesis, analytical characterization, and human CB_1 receptor binding studies of the chloroindole analogues of the synthetic cannabinoid MDMB-CHMICA. *Biomolecules* **2024**, *14* (11), 1414.
(40) de Oliveira, M. C.; Vides, M. C.; Lassi, D. L. S.; Torales, J.; Ventriglio, A.; Bombana, H. S.; Leyton, V.; Périco, C. A.; Negrão, A. B.; Malbergier, A.; et al. Toxicity of synthetic cannabinoids in K2/Spice: A systematic review. *Brain Sci.* **2023**, *13* (7), 990.
(41) Lee, C.; Yang, W.; Parr, R. G. Development of the Colle-Salvetti correlation-energy formula into a functional of the electron density. *Phys. Rev. B* **1988**, *37* (2), 785−789.
(42) Becke, A. D. Density-functional thermochemistry. III. The role of exact exchange. *J. Chem. Phys.* **1993**, *98* (7), 5648−5652.
(43) Becke, A. D. A new mixing of Hartree−Fock and local density-functional theories. *J. Chem. Phys.* **1993**, *98* (2), 1372−1377.
(44) Weigend, F.; Ahlrichs, R. Balanced basis sets of split valence, triple zeta valence and quadruple zeta valence quality for H to Rn: Design and assessment of accuracy. *Phys. Chem. Chem. Phys.* **2005**, *7* (18), 3297−3305.
(45) Feng, G.; Yamashita, M. Synthesis and reactivity of an alumanyl−tin species to form an Al,N-heteroallene derivative. *J. Am. Chem. Soc.* **2024**, *146* (42), 28653−28657.
(46) Li, P.-Y.; Liu, Y.; Wang, S.-J.; Liu, D.; Li, G.-Y. TDDFT study on a fluorescent probe for distinguishing analogous thiols based on smiles rearrangement. *Spectrochim. Acta A Mol. Biomol. Spectrosc.* **2024**, *304*, No. 123396.
(47) Dreuw, A.; Head-Gordon, M. Single-reference ab initio methods for the calculation of excited states of large molecules. *Chem. Rev.* **2005**, *105* (11), 4009−4037.
(48) Kondo, M. Singlet-triplet energy gap of multiresonant molecular systems: A double hybrid time-dependent density functional theory study. *Chem. Phys. Lett.* **2022**, *804*, No. 139895.
(49) Marenich, A. V.; Cramer, C. J.; Truhlar, D. G. Universal solvation model based on solute electron density and on a continuum model of the solvent defined by the bulk dielectric constant and atomic surface tensions. *J. Phys. Chem. B.* **2009**, *113* (18), 6378−6396.
(50) Zhang, I. Y.; Su, N. Q.; Brémond, É. A. G.; Adamo, C.; Xu, X. Doubly hybrid density functional xDH-PBE0 from a parameter-free global hybrid model PBE0. *J. Chem. Phys.* **2012**, *136* (17), 174103.
(51) Schäfer, A.; Huber, C.; Ahlrichs, R. Fully optimized contracted Gaussian basis sets of triple zeta valence quality for atoms Li to Kr. *J. Chem. Phys.* **1994**, *100* (8), 5829−5835.
(52) Duan, N.; Wu, X.; Yang, S.; Tian, H.; Sun, B. A novel large-stokes shift fluorescent probe for visual recognition of $Fe^{3+/2+}$ and its strip applications. *J. Photochem. Photobiol. A Chem.* **2024**, *454*, No. 115704.
(53) Roohi, H.; Pouryahya, T. Tuning the photophysical properties of ESIPT active unsymmetrical azine dyes by the change in the substituent and solvent: TD-PBE0 and TD-CAM-B3LYP studies. *Mol. Syst. Des. Eng.* **2024**, *9* (6), 625−648.
(54) Duarte, H. A.; Heine, T.; Seifert, G. DFT × TB − a unified quantum-mechanical hybrid method. *Theor. Chem. Acc.* **2005**, *114* (1), 68−75.
(55) Grimme, S.; Bannwarth, C.; Shushkov, P. A robust and accurate tight-binding quantum chemical method for structures, vibrational frequencies, and noncovalent interactions of large molecular systems parametrized for all spd-block elements (Z = 1−86). *J. Chem. Theory Comput.* **2017**, *13* (5), 1989−2009.
(56) Frisch, M. J.; Trucks, G. W.; Schlegel, H. B.; Scuseria, G. E.; Robb, M. A.; Cheeseman, J. R.; Scalmani, G.; Barone, V.; Petersson, G. A.; Nakatsuji, H.et al., *Gaussian 09*, Rev C.01, Gaussian, Inc.: Wallingford CT, 2016.
(57) Lu, T.; Chen, F. Quantitative analysis of molecular surface based on improved Marching Tetrahedra algorithm. *J. Mol. Graph. Model.* **2012**, *38*, 314−323.
(58) Zhang, J.; Lu, T. Efficient evaluation of electrostatic potential with computerized optimized code. *Phys. Chem. Chem. Phys.* **2021**, *23* (36), 20323−20328.
(59) Lu, T.; Chen, Q. A simple method of identifying π orbitals for non-planar systems and a protocol of studying π electronic structure. *Theor. Chem. Acc.* **2020**, *139* (2), 25.
(60) Lefebvre, C.; Rubez, G.; Khartabil, H.; Boisson, J.-C.; Contreras-García, J.; Hénon, E. Accurately extracting the signature of intermolecular interactions present in the NCI plot of the reduced density gradient versus electron density. *Phys. Chem. Chem. Phys.* **2017**, *19* (27), 17928−17936.
(61) Lu, T.; Chen, F. Multiwfn: A multifunctional wavefunction analyzer. *J. Comput. Chem.* **2012**, *33* (5), 580−592.
(62) Lu, T. A comprehensive electron wavefunction analysis toolbox for chemists, Multiwfn. *J. Chem. Phys.* **2024**, *161* (8), No. 082503.
(63) Humphrey, W.; Dalke, A.; Schulten, K. VMD: Visual molecular dynamics. *J. Mol. Graph.* **1996**, *14* (1), 33−38.
(64) Dalpozzo, R. Strategies for the asymmetric functionalization of indoles: an update. *Chem. Soc. Rev.* **2015**, *44* (3), 742−778.

https://doi.org/10.1021/acsomega.5c00540
ACS Omega 2025, 10, 14306−14315

(65) Bayly, C. I.; Cieplak, P.; Cornell, W.; Kollman, P. A. A well-behaved electrostatic potential based method using charge restraints for deriving atomic charges: the RESP model. *J. Phys. Chem.* **1993**, *97* (40), 10269−10280.

https://doi.org/10.1021/acsomega.5c00540
ACS Omega 2025, 10, 14306−14315